Journal of Physics and Chemistry of Solids 158 (2021) 110255

Contents lists available at ScienceDirect

Journal of Physics and Chemistry of Solids

journal homepage: www.elsevier.com/locate/jpcs

Three-dimensional $NiCo_2O_4$ nanosheets and nanoflowers electrodeposited with palladium nanoparticles on nickel foam for the hydrogen evolution reaction

Bingcheng Sun [a,1], Fengjuan Miao [a,1,*], Bairui Tao [a,**], Yanchun Wang [a], Yu Zang [b], Paul K. Chu [c]

[a] College of Communications and Electronics Engineering, Qiqihar University, Heilongjiang, 161006, China
[b] College of Materials Science and Engineering, Qiqihar University, Wenhua Street 42, Qiqihar, China
[c] Department of Physics, Department of Materials Sciences and Engineering, And Department of Biomedical Engineering, City University of Hong Kong, Tat Chee Avenue, Kowloon, Hong Kong, China

ARTICLE INFO

Keywords:
3D structure
Alkaline
Hydrogen evolution reaction (HER)
Nickel cobalt oxide
Nickel foam

ABSTRACT

By combining $NiCo_2O_4$ with good hydrogen evolution reaction (HER) properties and palladium (Pd) nanoparticles with excellent conductivity, a highly efficient and stable catalyst is prepared for HER. The $NiCo_2O_4$ nanosheets and $NiCo_2O_4$ nanoflowers are produced on the nickel foam (NF) with a large specific surface area by a one-step hydrothermal method and the $NiCo_2O_4$ nanoflowers are uniformly distributed in the $NiCo_2O_4$ nanosheets to form a three-dimensional (3D) electrode. Compared to conventional $NiCo_2O_4$, the 3D $NiCo_2O_4$ electrode provides more active sites (Ni and Co) for oxygen adsorption thus reducing the energy required to break H–O bonds to promote HER. When $NiCo_2O_4$/NF is combined with Pd nanoparticles (Pd/$NiCo_2O_4$/NF), the HER performance is improved greatly because of the synergistic effects rendered by the 3D structure of $NiCo_2O_4$ and Pd nanoparticles. The overpotential of Pd/$NiCo_2O_4$/NF is 69 mV at a current density is 10 mA/cm^2 and it is stable for 10 h in alkaline environments. The materials design and properties provide useful information for future development of commercial hydrogen production.

1. Introduction

Burning of fossil fuels is producing deleterious environmental effects and clean energy sources are important to the modern society [1–3]. Hydrogen energy (H_2) is a promising alternative to fossil fuel [4,5] because combustion of H_2 gives out more energy than most other substances and the byproduct of water does not pose environmental threats. One of the desirable means to produce pure hydrogen is water electrolysis or water splitting, which involves two basic semi-reactions: the hydrogen evolution reaction (HER) and oxygen evolution reaction (OER) [6]. The main obstacle impeding large-scale production of H_2 by water splitting is the lack of efficient and stable catalysts. Platinum (Pt) is the best HER catalyst but has disadvantages such as the high cost and natural scarcity. Some metals can replace Pt based on the volcanic diagram and Pd also delivers good HER performance when combined with other substances [7]. However, although Pd in combination with metals can increase the HER activity of HER, the overpotential tends to be high and so more energy is needed to break H–O bonds in water dissociation.

Although Pd nanoparticles can improve the HER activity of hydroxyl compounds, the HER activity also depends on the other characteristics of the electrode materials. Transition metal oxides containing Ni, Mn, and Co have been suggested to be alternative electrode materials [8] and mixed transition metal oxides such as $NiCo_2O_4$ and $MnCo_2O_4$ have also been proposed for HER [9]. For example, Ni^{2+} replaces Co^{2+} in the spinel Co_3O_4 and cubic crystal of CoO to form $NiCo_2O_4$ and $NiCoO_2$, respectively [10,11] and the HER properties of $NiCoO_2$ with different morphologies such as nanoflakes, nanoparticles, nanowires, and nanoflowers have been studied. For substrates, NF is a good choice due to its high specific surface area and low cost. For example, Zhang et al. grew Co_2MnO_4 on NF for hydrogen evolution [12]. In addition, changing the structure of the sample can also optimize the hydrogen evolution performance of the sample. For example, the 3D Multipods structure grown

* Corresponding author.
** Corresponding author.
E-mail addresses: miaofengjuan@163.com, miaofengjuan@qqhru.edu.cn (F. Miao), tbr_sir@163.com (B. Tao).
[1] Bingcheng Sun and Fengjuan Miao are co-first authors.

https://doi.org/10.1016/j.jpcs.2021.110255
Received 5 May 2021; Received in revised form 1 July 2021; Accepted 10 July 2021
Available online 13 July 2021

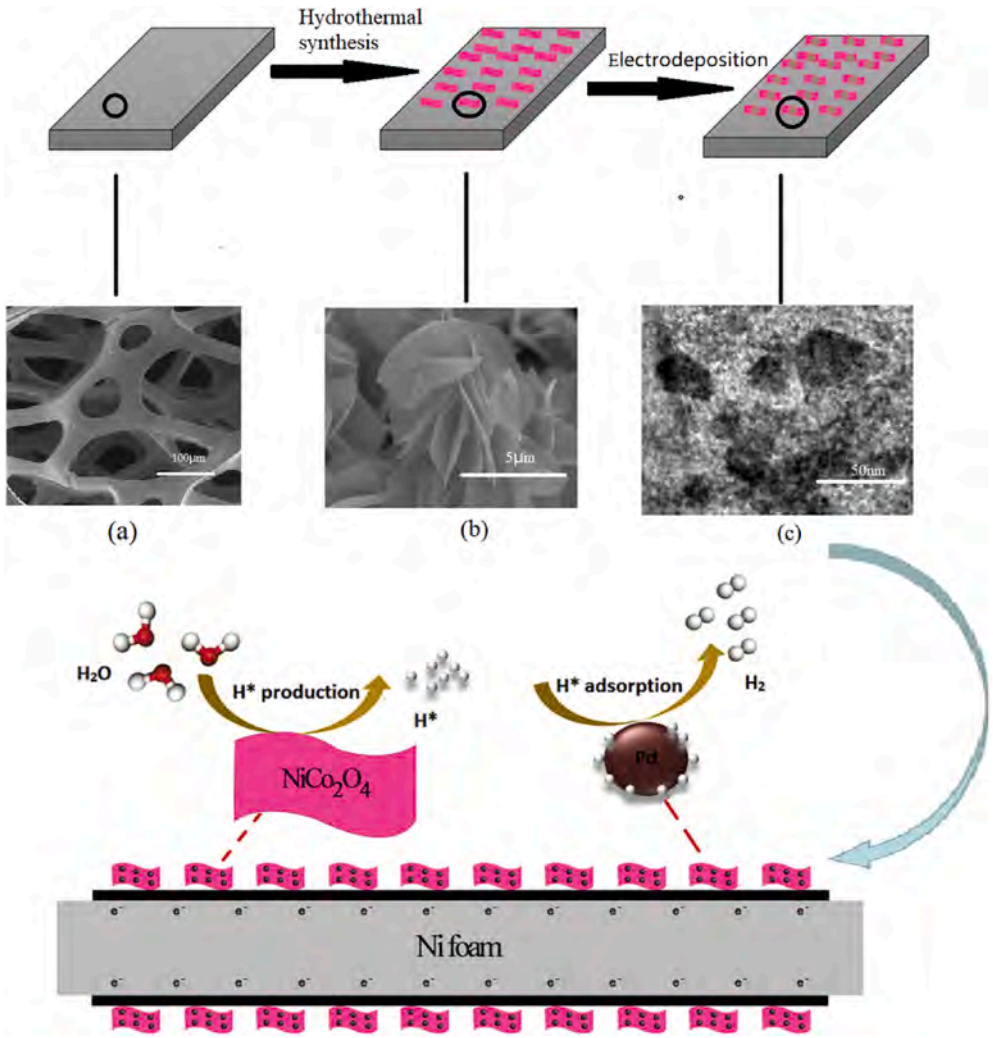

Fig. 1. Structure of $Pd/NiCo_2O_4/NF$ and corresponding HER process.

on NF by Chen et al. is used for hydrogen evolution [13], Feng et al. optimized the hydrogen evolution electrode by modifying the electrode with Pd [14].

In this work, a three-dimensional (3D) $NiCo_2O_4$ structure is designed to enhance the HER activity. Orderly $NiCo_2O_4$ nanoflowers are prepared on nanosheets by a one-step hydrothermal method and Pd nanoparticles are incorporated into the 3D $NiCo_2O_4$ structure to produce synergistic effects. In addition to providing a large number of active sites for oxygen adsorption, the energy needed to break H–O bonds is reduced to improve the HER activity.

2. Materials and methods

2.1. The experimental items

The NF was purchased from Guang Sheng Jia New Materials Co., Ltd., China and palladium chloride ($PdCl_2$) was obtained from Henan Dashun Industrial Corporation. Cobalt nitrate ($Co(No_3)_2{\cdot}6H_2O$), nickel nitrate ($Ni(No_3)_2{\cdot}6H_2O$), urea (H_2NCONH_2), and ammonium fluoride (NH_4F) were acquired from Beijing Chemical Corporation and KOH was obtained from Aladdin Ltd., Shanghai, China. All the chemicals were used without purification and processing and deionized distilled water was used in the experiments.

2.2. Preparation of $NiCo_2O_4/NF$

The NF pieces with dimensions of 10 mm × 10 mm x 1.5 mm were cleaned ultrasonically with deionized water, hydrochloric acid, deionized water, alcohol and deionized water sequentially and dried in an oven at 60 °C for 30 min. 0.3877 g of nickel nitrate hexahydrate, 0.7761 g of cobalt nitrate hexahydrate, and 0.4805 g of urea were added to 80 mL of deionized water and sonicated for 15 min to obtain a clear pink solution. The solution was put into a reactor in which the NF was put on the inner wall at an angle of 45°. The sealed reactor was put in a water bath at 120 °C for 3 h. After natural cooling to room temperature, the NF was rinsed with deionized water, put on a silicon wafer, and annealed at 350 °C for 2 h to produce $NiCo_2O_4/NF$.

2.3. Synthesis of $Pd/NiCo_2O_4/NF$

$Pd/NiCo_2O_4/NF$ was prepared by electrochemical deposition. 19.62 mg of $PdCl_2$, 0.75 g of NH_4Cl, and 2.34 g of EDTA were placed in 40 mL of deionized water and the pH was adjusted to 8 by addition of NH_4OH. The sample was subjected to electrodeposition at a current density of 10 mA/cm^2 for 20 min, rinsed with deionized water, and dried at 60 °C for 30 min.

2.4. Materials characterization

Scanning electron microscopy (SEM, Tescan MIRA 3XMU), field-

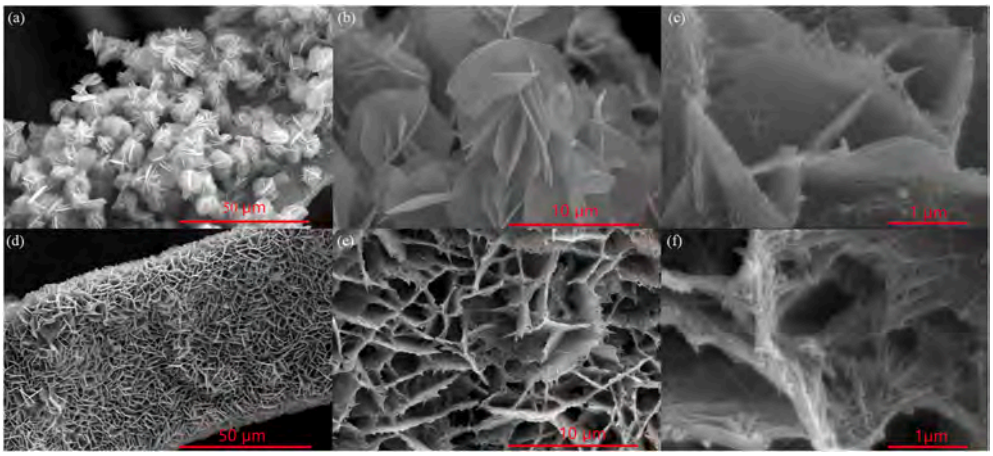

Fig. 2. (a–e) SEM images of Pd/$NiCo_2O_4$/NF at different magnifications.

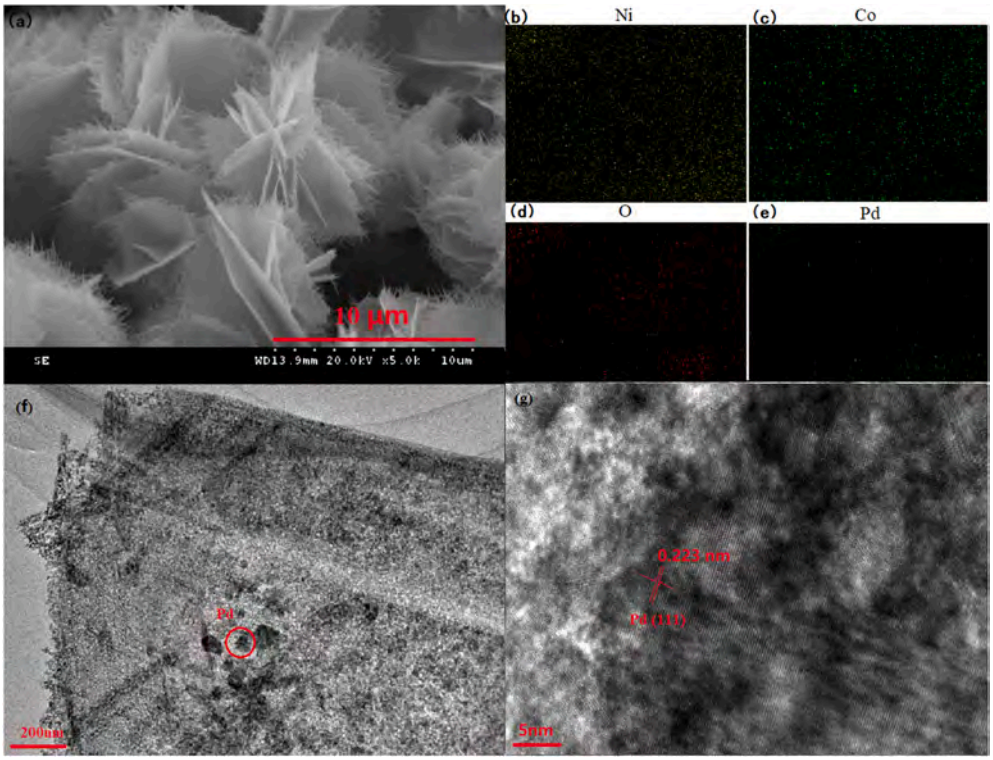

Fig. 3. (a) Partial SEM image of Pd/$NiCo_2O_4$/NF; (b ~ e) Pd, Ni, Co, and O distributions of Pd/$NiCo_2O_4$/NF; (f) TEM micrographs of Pd/$NiCo_2O_4$/NF; (g) HR-TEM micrographs of Pd/$NiCo_2O_4$/NF.

emission transmission electron microscopy (TEM/HRTEM, JEM 2100F), X-ray photoelectron spectroscopy (XPS, ESCALAB250Xi), and X-Ray diffraction (XRD) were performed to characterize the morphology, composition, and structure of the samples. Elemental composition was determined by the inductively coupled plasma mass-spectrometer (ICP-MS, Elan DRC II PerkinElmer SCIEX).

2.5. Electrochemical measurements

An electrochemical workstation (Shanghai Chenhua CHI760D) was employed to monitor hydrogen evolution in 0.1 M aqueous KOH. The counter and reference electrodes were a platinum foil and saturated calomel electrode, respectively. The polarization curves (LSV) were acquired at a scanning rate of 10 mV/s and the Tafel slope was determined from the polarization curve. Electrochemical impedance spectroscopy (EIS) was carried out in the frequency range between 100 kHz and 0.01 Hz and CV was conducted to determine the active surface area of the samples.

3. Results and discussion

3.1. Characterization

Fig. 1 shows the 3D structure of Pd/$NiCo_2O_4$/NF and HER. Many sites adsorb oxygen due to H–O bonds and a large amount of H_{ads} is converted into H_2 while Pd promotes ion transport in the reaction. The morphology of Pd/$NiCo_2O_4$/NF is examined by scanning electron microscopy (SEM). Fig. 2(a) shows that many $NiCo_2O_4$ nanoflowers with a diameter of about 6 μm are formed on the NF and the high-magnification SEM images of the $NiCo_2O_4$ nanoflowers are depicted in Fig. 2(b) and

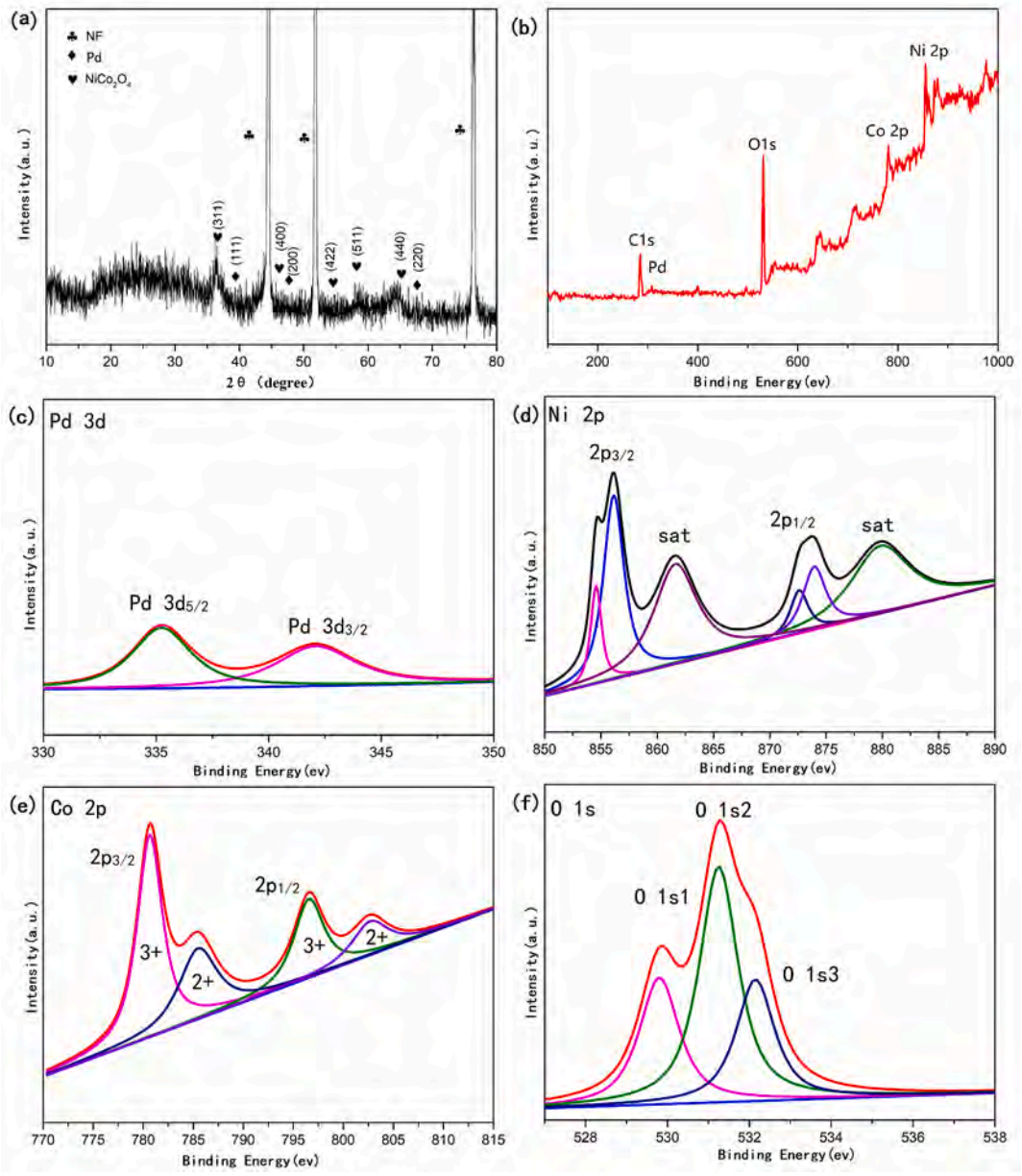

Fig. 4. (a) XRD of Pd/$NiCo_2O_4$/NF; (b) XPS of Pd/$NiCo_2O_4$/NF; (c) Pd 3d, (d) Ni 2p, (e) Co 2p and (f) O 1s regions.

(c). The $NiCo_2O_4$ nanoflowers are composed of many interconnected nanoflakes. Fig. 2(d ~ f) show the magnified images of the $NiCo_2O_4$ nanoflakes on NF and these nanoflakes are loose and evenly distributed. However, the size of these nanoflakes is different from that of the nanoflowers. The $NiCo_2O_4$ nanoflowers prepared on aligned nanoflakes provide abundant sites for oxygen attachment to reduce the energy required to break H–O bonds. Pd/$NiCo_2O_4$/NF is analyzed by Mapping as shown in Fig. 3(b)~(e) shows that Ni, Co, O and Pd are distributed evenly. Fig. 3(f) shows that the nanoflakes are separated from the sample after sonication due to loose agglomeration, we can see that the diameter of Pd is about 50 nm. Fig. 3(g) shows the HRTEM micrograph. It can be seen that the lattice fringe of 0.223 nm is consistent with the Pd (111) plane.

The composition and structure of Pd/$NiCo_2O_4$/NF is determined by XRD. In Fig. 4(a), the obvious peaks at $2\theta = 44.8°$, 52.3°and 76.8° are assigned to the NF. The peaks at $2\theta = 40.2°$, 46.9°, 68.4° are indexed to the crystal planes (111), (200) and (220) of Pd (JCPDS 46e1043). The other sharp peaks at $2\theta = 18.6°$, 32.6°, 37.3° and 62.3° belong to the crystal planes (311), (400), (422), (511) and (440) of $NiCo_2O_4$ (JCPDS 20e0781). The results indicate that Pd/$NiCo_2O_4$/NF has been successfully obtained. Fig. 4(b) presents the spectrum of Pd/$NiCo_2O_4$/NF revealing O 1s, Pd, Ni 2p, and Co 2p peaks. As shown in Fig. 4(c), the two rotation orbits (Pd^0 and Pd^{2+}) constitute the 3D spectrum of Pd and the peaks of Pd^0 and Pd^{2+} are located at 342.5 eV and 377.1 eV, respectively. Fig. 4(d) reveals Ni^{2+} and Ni^{3+} and Co^{2+} and Co^{3+} are observed from Fig. 4(e). Fig. 4(f) shows the O 1s1 peak at 529.6 eV, defect oxygen O 1s2 peak at 531.3 eV, and hydroxyl O 1s3 peak at 533.5 eV. O 1s1 exists in $NiCo_2O_4$ and O 1s3 exists in water.

3.2. Electrochemical assessment of HER activity

To study the hydrogen evolution activity of Pd/$NiCo_2O_4$/NF under alkaline conditions, three electrodes including the clean NF, one covered with Pd on NF (Pd/NF), and one covered with $NiCo_2O_4$ on NF ($NiCo_2O_4$/NF) are compared. The three-electrode test was carried out in 0.1 M KOH with the platinum electrode as the counter electrode, Pd/$NiCo_2O_4$/NF, NF, $NiCo_2O_4$/NF, or Pd/NF as the working electrode, and saturated calomel electrode as the reference electrode. The current density and

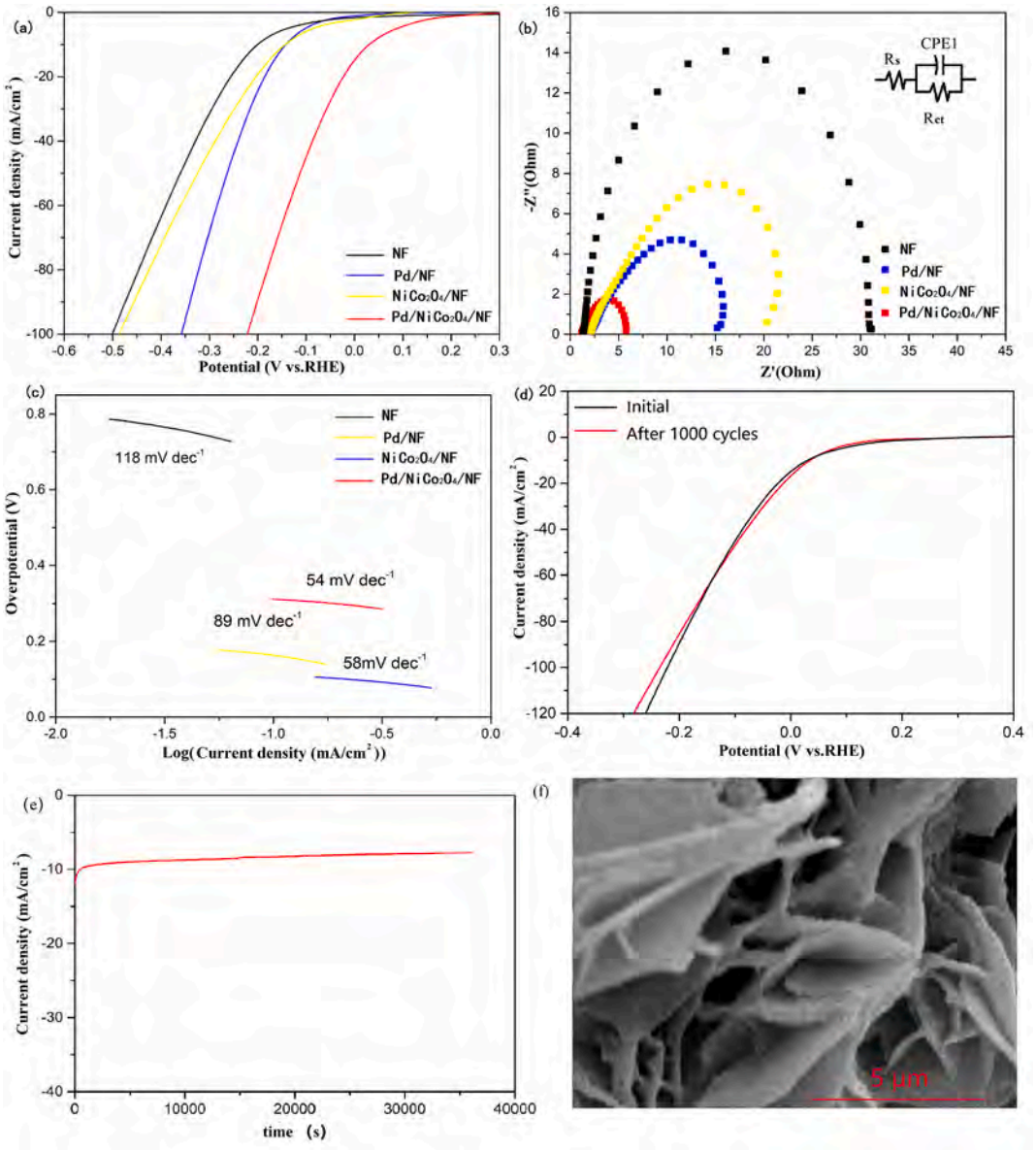

Fig. 5. (a) LSV of NF, Pd/NF, $NiCo_2O_4$/NF, and Pd/$NiCo_2O_4$/NF;(b) Nyquist plots of NF, Pd/NF, $NiCo_2O_4$/NF, and Pd/$NiCo_2O_4$/NF; (c) Tafel plots of NF, Pd/NF, $NiCo_2O_4$/NF, and Pd/$NiCo_2O_4$/NF; (d) Polarization initially and after 1000 cycles of Pd/$NiCo_2O_4$/NF; (e) chronoamperometric curves; (f) SEM images of Pd/$NiCo_2O_4$/NF after chronoamperometric curves of 10 h.

overpotential of the electrode are derived from the LSV in Fig. 5(a). The current densities increase with potentials. The overpotential (192 mV) of the pristine NF is the highest at the current density of 10 mA/cm^2. When NF is covered by Pd or 3D $NiCo_2O_4$, the overpotentials decrease to 141 mV and 143 mV respectively. Pd nanoparticles improve the electrical conductivity and the 3D $NiCo_2O_4$ provides more active sites for oxygen adsorption. Pd/$NiCo_2O_4$/NF shows the lowest potential of 69 mV, due to the synergistic effects of the 3D structure of $NiCo_2O_4$ and Pd. The content of Pd in the electrodes (Pd/$NiCo_2O_4$/NF and Pd/NF) were investigated by ICP-MS. The loading mass of Pd nanoparticles on the Pd/$NiCo_2O_4$/NF electrode was 0.44 mg (0.44 mg/cm^2), which was similar to that of the Pd/NF electrode 0.43 mg (0.43 mg/cm^2).

Electrochemical impedance spectroscopy (EIS) is carried to study the mechanism. The Nyquist plots of Pd/$NiCo_2O_4$/NF, Pd/NF, $NiCo_2O_4$/NF, and NF are obtained at ɧ = 100 mV and between 100 kHz and 0.01 Hz, as shown in Fig. 5(b). The Nyquist equivalent circuit is shown in the inset in Fig. 5(b), where R_s is the equivalent resistance of the electrolyte, CPE1 is the constant phase element, and R_{ct} is the charge transfer resistance. The resistance of the electrolyte is basically unchanged and the main influence is from R_{ct}. The fitted curve resembles a semicircle and generally speaking, a smaller diameter of the semicircle indicates smaller resistance. The Nyquist results show that Pd/$NiCo_2O_4$/NF has the smallest resistance of 5.53 Ω in comparison with NF (29.7 Ω), $NiCo_2O_4$/NF (17.8 Ω), and Pd/NF (14.7 Ω). The results are in line with LSV, indicating that Pd/$NiCo_2O_4$/NF has the fastest charge transfer rate compared to Pd/NF, $NiCo_2O_4$/NF, and NF.

The Tafel slopes are determined from the linear region of the Tafel plots according to the Tafel equation: η = a + b log i (where η is the overpotential, b is the Tafel slope, and i is the current density) and a represents the overpotential when the current density is a single value. The Tafel slope is related to the properties of the electrode materials, electrode surface state, solution composition, temperature and other factors. According to the value of the a, the difficulty in the electron transfer steps in different electrode systems can be compared. The Tafel slopes of Pd/$NiCo_2O_4$/NF (54 mV/dec), $NiCo_2O_4$/NF (58 mV/dec), Pd/NF (89 mV/dec) and NF (118 mV/dec) shown in Fig. 5(c) reveal that

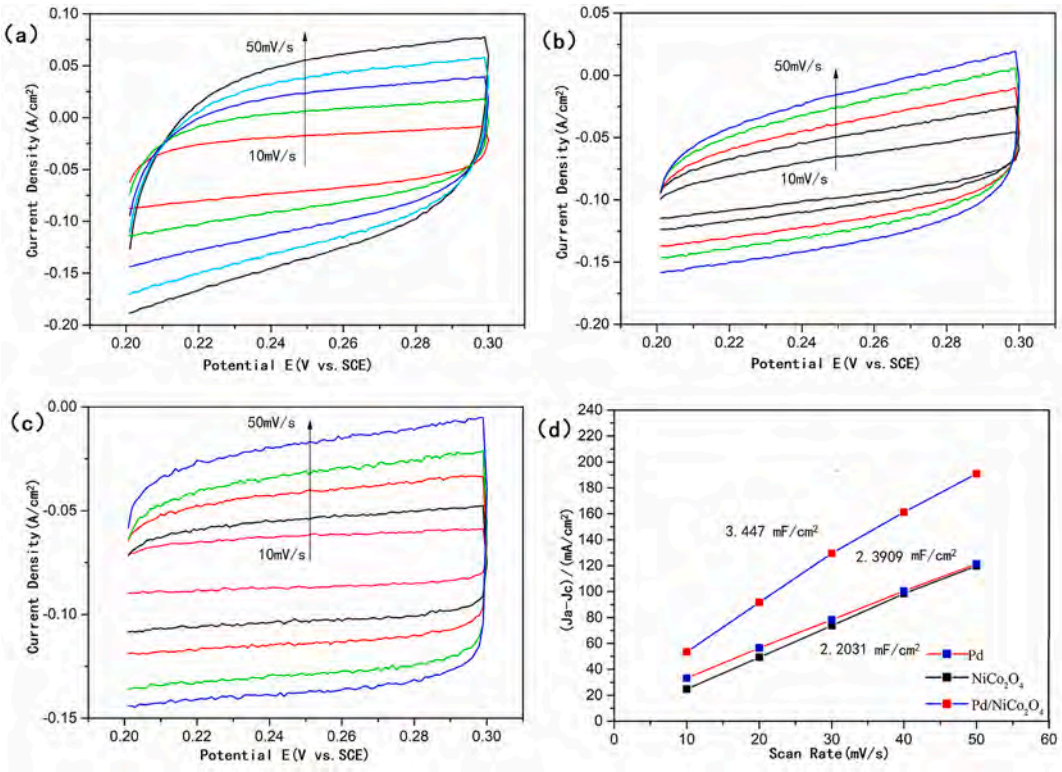

Fig. 6. CV of (a) $Pd/NiCo_2O_4$/NF, (b) $NiCo_2O_4$/NF, and (c) Pd/NF; (d) Linear fitting of the capacitive currents at scanning rates from 10 mV/s to 50 mV/s.

kinetically, $Pd/NiCo_2O_4$/NF exhibits enhanced activity. The HER mechanism involves three steps (Tafel, Heyrovsky, and Volmer):

Volmer reaction : $H_2O + e^- \rightarrow H_{ads} + OH^-$

Heyrovsky reaction : $H_2O + H_{ads} + e^- \rightarrow OH^- + H_2$

Tafel reaction : $H_{ads} + H_{ads} \rightarrow H_2$

The Volmer reaction is an essential step in hydrogen evolution and occurs at the Tafel slope of 120 mV/dec, whereas those of the Heyrovsky and Tafel reactions are at 40 mV/dec and 30 mV/dec, respectively. The Tafel slopes of $Pd/NiCo_2O_4$/NF (54 mV/dec), $NiCo_2O_4$/NF (58 mV/dec), Pd/NF (89 mV/dec), and NF (118 mV/dec) are between 40 mV/dec and 120 mV/dec, indicating that the Volmer reaction and Heyrovsky reaction are the main reactions as consistent with the LSV results.

CV cycling is performed to study the stability of $Pd/NiCo_2O_4$/NF. Fig. 5(d) shows the polarization curves of $Pd/NiCo_2O_4$/NF for the initial cycle and after 1000 CV cycles at a rate of 100 mV/s in the range between 1.0 V and 1.4 V. There is no significant change in the activity of $Pd/NiCo_2O_4$/NF during cycling. The black line represents the initial data and the potential is 222 mV when the current density reaches 100 mA/cm^2. As shown in the red line, the potential is 227 mV when the current density reaches 100 mA/cm^2 after 1000 cycles. The small change indicates that $Pd/NiCo_2O_4$/NF essentially retains the original activity. In order to explore the stability of the electrode, it is necessary to test the time evolution of the electrode and the results are shown in Fig. 5(e). The input voltage is the open circuit voltage and the initial slope indicates that it takes some time to reach a stable state. In the next 10 h, the current density is basically stable and it can thus be inferred that $Pd/NiCo_2O_4$/NF has good chemical activity and stability. Fig. 5(f) shows that the morphology and structure of the $Pd/NiCo_2O_4$/NF nanosheet arrays are main tained after 10 h.

To determine the activity of the specific surface area, CV is carried out and the results are displayed in Fig. 6(a)–6(c). CV is conducted on Pd/NF, $NiCo_2O_4$/NF and $Pd/NiCo_2O_4$/NF at different rates (10–50 mV/s) in the voltage range of 0.2–0.3 V. The diagram shows of rectangles in different regions. Each rectangle represents a stable state at the same scanning rate by trial and error. The nonuniform line is caused by the narrow testing range but does not affect the experimental analysis. The larger rectangular area shows the greater specific surface area on the electrode and a greater activity leads to higher energy storage capacity. Therefore, with increasing scanning rates, the energy storage effect of the electrode is better. For example, at a scanning rate of 50 mV/s and voltage of 0.25V, the current density of $Pd/NiCo_2O_4$/NF is positive but that of $Pd/NiCo_2O_4$/NF is negative. This is observed at any scanning rate and therefore, $Pd/NiCo_2O_4$/NF has a bigger active specific surface area and better energy storage capacity than the others. Fig. 6(d) shows the Cdl values of $Pd/NiCo_2O_4$/NF (3.447 mF/cm^2), Pd/NF (2.3909 mF/cm^2), and $NiCo_2O_4$/NF (2.2031 mF/cm^2) and the larger Cdl indicates better catalytic properties for $Pd/NiCo_2O_4$/NF and larger greater electrochemical active surface area in HER.

In order to illustrate the advantages of $Pd/NiCo_2O_4$/NF in HER, a comparison is made with other electrodes as shown in Table 1. For example, Xiao et al. have prepared $NiCo_2O_4$ nanosheets on NF for HER but the effects are not as good as those of the 3D $NiCo_2O_4$ nanostructure in our study. Furthermore, the 3D $NiCo_2O_4$ nanostructure is easier to fabricate than the single-layer $NiCo_2O_4$ nanosheets and penetration of the electrolyte OH^- is also facilitated in $NiCo_2O_4$ for better HER.

Table 1
Comparison of the HER performance of various catalysts reported in the literature.

Catalyst	Overpotential (mV)	Tafel (mV/dec)	ref
$NiCo_2O_4$/NF	164	107	[15]
NiFe/NF	148	110	
NiFe/$NiCo_2O_4$/NF	105	88	
Pd/MOF	105	85	[16]
Ag@PdAg	93	83	[17]
Pd/3D-N-Rgo	92.9	136	[18]
Pt/c	44	30	[19]
Pt/NF	16.6	87.9	[20]
$Pd/NiCo_2O_4$/NF	69	54	This work
$NiCo_2O_4$/NF	143	58	

Although other researchers have used Pd nanoparticles to improve the HER properties, their materials are still relatively expensive and the performance is typically not as good as that of our 3D $NiCo_2O_4$. In fact, the performance of our electrode is second only to that of the Pt/c and Pt/NF electrode.

4. Conclusion

$NiCo_2O_4$ nanoflowers with a diameter of about 6 μm are prepared on $NiCo_2O_4$ nanoflakes coated on NF to obtain 3D $NiCo_2O_4$/NF, which is then modified with Pd nanoparticles by electrodeposition to produce Pd/$NiCo_2O_4$/NF. The Pd/$NiCo_2O_4$/NF electrode does not require a binder. In the electrochemical assessment using the conventional three-electrode configuration, Pd/$NiCo_2O_4$/NF shows an overpotential of 69 mV at a current density of 10 mA/cm^2 as well as the smallest Tafel slope (54 mV/dec). It is because the $NiCo_2O_4$ nanoflowers prepared on the aligned nanoflakes provide more active sites (Ni and Co) for oxygen adsorption and reduce the energy required to break H–O bonds. The Pd nanoparticles also decrease the energy required to break up hydroxide groups. Our experimental results show that the 3D $NiCo_2O_4$ structure with Pd nanoparticles has higher HER activity and the materials design and excellent performance reported in this paper bode well for the design of high-performance electrode materials.

Declaration of competing interest

The authors declare that they have no known competing financial interests or personal relationships that could have appeared to influence the work reported in this paper.

Acknowledgements

We would like to thank the Engineering Research Center of Agricultural Multi-Dimensional Sensor Information Perception, Heilongjiang Province, and Heilongjiang Provincial Key Laboratory of Micro-Nano Sensor Component. This work was jointly supported by the Fundamental Research Funds in Heilongjiang Provincial Universities (Nos. 135109244, 135309115, 135309211, 135409104 and 135409423), Heilongjiang Science Foundation Project (JQ2019F003 and ZD2019F004), as well as City University of Hong Kong Strategic Research Grant (SRG) (No. 7005505).

References

[1] Yang, An, Yuanyuan, et al., Improving the photocatalytic hydrogen evolution of UiO-67 by incorporating Ce~(4+)-coordinated bipyridinedicarboxylate ligands[J], Sci. Bull. 64 (20) (2019) 38–45.

[2] L. Gidi, J. Honores, José Ibarra, et al., Study of the hydrogen evolution reaction using ionic liquid/cobalt porphyrin systems as electro and photoelectrocatalysts [J], Catalysts 10 (2) (2020) 239.

[3] H. Wang, X. Hu, Y. Ma, et al., Nitrate-group-grafting-induced assembly of rutile TiO_2 nanobundles for enhanced photocatalytic hydrogen evolution[J], Chin. J. Catal. 41 (1) (2020) 95–102.

[4] M.M. Borisova-Mubarakshina, A.A. Tsygankov, T. Tomo, et al., International conference on "photosynthesis and hydrogen energy Research for sustainability-2019": in honor of tingyun kuang, anthony larkum, cesare marchetti, and kimiyuki satoh[J], Photosynth. Res. 146 (1) (2020) 5–15.

[5] Y. Li, K. Luo, Flexible cupric oxide photocathode with enhanced stability for renewable hydrogen energy production from solar water splitting[J], RSC Adv. 9 (15) (2019) 8350–8354.

[6] S. Shiva, Kumar, et al., Phosphorus-doped carbon nanoparticles supported palladium electrocatalyst for the hydrogen evolution reaction (HER) in PEM water electrolysis[J], Ionics 24 (10) (2018) 3113–3121.

[7] T. Takashima, T. Suzuki, H. Irie, Electrochemical reduction of carbon dioxide to formate on palladium-copper alloy nanoparticulate electrode[J], Electrochemistry -Tokyo- 87 (2) (2019) 134–138.

[8] P. Ilanchezhiyan, G.M. Kumar, C. Siva, et al., Evidencing enhanced oxygen and hydrogen evolution reactions using In-Zn-Go ternary transition metal oxide nanostructures: a novel bifunctional electrocatalyst[J], Int. J. Hydrogen Energy 44 (41) (2019) 23081–23090.

[9] X. Du, H. Su, X. Zhang, 3D $MnCo_2O_4$@CoS nanoarrays with different morphologies as an electrocatalyst for oxygen evolution reaction[J], Int. J. Hydrogen Energy 44 (39) (2019) 21637–21650.

[10] Bin Liu, Junye Cheng, Hui-Qing Peng, et al., In situ nitridated porous nanosheet networked Co_3O_4 –Co_4N heteronanostructures supported on hydrophilic carbon cloth for highly efficient electrochemical hydrogen evolution[J], J. Mater. Chem. 7 (2) (2019) 775–782.

[11] S.S. Yi, B.R. Wulan, J.M. Yan, et al., Highly efficient photoelectrochemical water splitting: surface modification of cobalt-phosphate-loaded Co_3O_4/Fe_2O_3 p-n heterojunction nanorod arrays[J], Adv. Funct. Mater. 29 (11) (2019) 1801902.1–1801902.9.

[12] R.L. Zhang, J.J. Feng, Y.Q. Yao, et al., Straw-like phosphorus-doped Co_2MnO_4 nanoneedle arrays supported on nickel foam for high-efficiency hydrogen evolution reaction in wide pH range of electrolytes[J], Appl. Surf. Sci. 548 (2021) 149280.

[13] A. Hyc, A. Hjn, H.A. Zhu, et al., Simple fabrication of trimetallic platinum-nickel-cobalt hollow alloyed 3D multipods for highly boosted hydrogen evolution reaction - ScienceDirect[J], J. Colloid Interface Sci. 570 (2020) 205–211.

[14] R.L. Zhang, J.J. Duan, L.P. Mei, et al., Facile synthesis of porous iridium-palladium-plumbum wire-like nanonetworks with boosted catalytic performance for hydrogen evolution reaction[J], J. Colloid Interface Sci. 580 (2020) 99–107.

[15] Changlong, Xiao, Yibing, et al., Bifunctional porous NiFe/$NiCo_2O_4$/Ni foam electrodes with triple hierarchy and double synergies for efficient whole cell water splitting[J], Adv. Funct. Mater. 26 (20) (2016) 3515–3523.

[16] Takanori, Miyake, Shun, et al., Regioselective hydrogenation of trans-1-Phenyl-1,3-butadiene on modified Pd/MOF catalysts[J], J. Jpn. Petrol. Inst. 63 (2) (2020) 96–101.

[17] R. Ma, Y. He, J. Feng, et al., A facile synthesis of Ag@PdAg core-shell architecture for efficient purification of ethene feedstock[J], J. Catal. 369 (2019) 440–449.

[18] P.J. Schafer, L.A. Kibler, Incorporation of Pd into Au (111): enhanced electrocatalytic activity for the hydrogen evolution reaction[J], Phys. Chem. Chem. Phys. 12 (46) (2010) 15225–15230.

[19] A. Kuriganova, N. Faddeev, M. Gorshenkov, et al., A comparison of "Bottom-Up" and "Top-Down" approaches to the synthesis of Pt/C electrocatalysts[J], Processes 8 (8) (2020) 947.

[20] L. Huang, Y. Hou, Z. Yu, et al., Pt/Fe-NF electrode with high double-layer capacitance for efficient hydrogen evolution reaction in alkaline media[J], Int. J. Hydrogen Energy 42 (15) (2017) 9458–9466.